J. Phys. B: At. Mol. Opt. Phys. **29** (1996) 5143–5161. Printed in the UK

Experimental studies of fusion and fragmentation of fullerenes

Frank Rohmund, Alexei V Glotov, Klavs Hansen and Eleanor E B Campbell

Max-Born-Institut für Nichtlineare Optik und Kurzzeitspektroskopie, Postfach 1107, D-12474 Berlin, Germany

Abstract. Energy dependences of the fusion cross section for the collisions $C_{60}^+ + C_{60}$, $C_{60}^+ + C_{70}$ and $C_{70}^+ + C_{70}$ have been measured. Fusion occurs for energies above a sharp energetic barrier V_B. The fusion barrier lies in the region between 60 and 80 eV and increases with increasing number of atoms participating in the collision. For energies beyond the barrier the fusion reaction cross section increases with collision energy to a maximum value and then decreases very rapidly. The highly excited fusion compound decays on the experimental timescale, and the resulting fragmentation pattern has been studied as a function of collision energy. For energies up to 200 eV the fragmentation behaviour can be modelled in terms of successive evaporation of C_2 units from the hot fusion product. At higher energies this model breaks down and another fragmentation mechanism has to be invoked. The overall results are in very good agreement with quantum molecular dynamics simulations and the predictions of simple phenomenological fusion models.

1. Introduction

Atomic and molecular collision experiments are powerful tools to help obtain insight into the dynamics of physical and chemical processes from a microscopic point of view. In recent years the interest in collisions between atomic clusters as examples of systems with a large but still finite number of degrees of freedom has been increasing. The dynamical behaviour of such systems is expected to show strong similarities to both heavy ion collisions (HIC) (Bock 1980) on the microscopic scale and to collisions between liquid droplets on the macroscopic scale (Schmidt and Lutz 1992, Schmidt *et al* 1992). Twenty orders of magnitude in size lie between these two cases. Atomic cluster–cluster collisions (CCC) should be able to, if not close this gap, at least give evidence for the validity of such an extreme range of scaling.

To date most of the investigations of CCC have been theoretical. The first studies of this kind by Schmidt and co-workers on collisions between sodium clusters, using density functional theory (Schmidt *et al* 1991, Schmidt and Lutz 1993), already showed the main features of the dynamics in CCC. The most striking characteristic is the appearance of a number of well defined reaction types. These are deep inelastic scattering (DIC), fusion, fragmentation and multi-fragmentation, which are expected to occur in this order with increasing collision energy. The fusion of sodium clusters has also been studied, using tight-binding methods (Zhang *et al* 1995). These authors investigated the influence of the collision energy and the impact parameter on the lifetime of the dimer formed in collisions. Fusion of liquid ^{3}He droplets (Guillemans *et al* 1993, 1995) and the growth of silicon particles from collisions of silicon clusters at thermal energies (Blaiston-Bajorat

0953-4075/96/215143+19$19.50

and Zachariah 1992) have also been investigated. Experimentally, however, the collision systems treated in these references are very difficult to realize and, to our knowledge, no experimental results have been obtained under well defined single collision conditions so far.

The availability of macroscopic amounts of fullerenes C_{60} and C_{70} made possible the experimental study of collision experiments with these clusters. Extensive work on collisions between fullerenes and atoms or molecules (e.g. Weiske *et al* 1991, Caldwell *et al* 1992, Wan *et al* 1992, Ehlich *et al* 1995) as well as surfaces (Beck *et al* 1991, Lill *et al* 1992) has been reported. Collision experiments in which C_1^+ (Christian *et al* 1992) or C_2^+ (Basir *et al* 1994) have been inserted into the C_{60} cage were carried out by the Anderson group. No activation barrier for these reactions could be estimated due to the accompanying exoergic electron transfer from the neutral C_{60} target to the projectile ion during the collision.

There are also a few investigations where interactions between clusters or CCC play a significant role. Martin *et al* (1993) produced clusters of C_{60}, which are bonded by van der Waals forces, in an aggregation source. Fusion of fullerenes has been observed in collisions of C_{60} with fullerite surfaces (Lill *et al* 1993). Coalescence reactions of fullerenes have also been observed upon laser desorption of bulk fullerenes (Yeretzian *et al* 1992, Mitzner *et al* 1996). Scheidemann *et al* carried out a CCC experiment in which they measured the scattering of sodium clusters in C_{60} vapour (Scheidemann *et al* 1994). Charge transfer processes between fullerene ions and neutrals in the thermal energy region (Javahery *et al* 1992) and in the keV region (Shen *et al* 1995) have been reported. Recently we determined cross sections for charge transfer reactions between C_{60}^{2+} and C_{60} (Rohmund and Campbell 1995) and $C_{60/70}^+$ and C_{60} (Rohmund and Campbell 1996) respectively.

The first observation of fusion and DIC in CCC between fullerenes under single collision conditions was reported by Campbell *et al* (1993). Almost simultaneously the first quantum molecular dynamics (QMD) simulations of C_{60}–C_{60} collisions were carried out (Seifert *et al* 1992). The theoretical work predicted fusion and DIC events in the range of collision energies between 150 and 500 eV which was nicely confirmed by the experimental work (Campbell *et al* 1993). The collision energies are those of the centre of mass frame, which will be used throughout this work unless otherwise stated. A somewhat more detailed theoretical treatment of the problem was carried out for $E = 500$ eV, where the simulations showed multi-fragmentation as a new decay mechanism and collective flow effects (Schmidt *et al* 1994), both in close analogy to HIC. For the same energy, mass and angular distributions of the collision products were also calculated (Schulte *et al* 1995). Besides the QMD-simulations several other, more approximate, methods have been applied to calculate fusion events in collisions between two C_{60} clusters. Zhang *et al* (1993) used a tight binding algorithm to calculate the fusion barrier for zero impact parameter as a function of the internal energy and the orientation of the reactants before the collision. As in the QMD results, the authors observed three different reaction channels (inelastic scattering, fusion and fragmentation). Classical MD simulations using empirical potentials were also applied to these collisions (Robertson *et al* 1995).

The theoretical treatments all predict the existence of a barrier for fusion which was seen to depend strongly on the internal energy before the collision. The values for the barrier given in the literature range between nearly 0 and 90 eV.

Recently we reported the energy dependence of the fusion cross section observed in collisions of C_{60}^+ with C_{60} (Rohmund *et al* 1996). The cross section displayed a threshold behaviour, consistent with the presence of an energetic barrier with the value 66 ± 7 eV. The cross section increased with collision energy to a maximum of $2\,\text{Å}^2$ at 130 eV and

dropped sharply to zero at higher collision energies. The data were analysed using a model which combined the fusion barrier with a simple absorbing sphere model. This procedure enabled us to extract a value for the fusion probability and the maximum impact parameter (or angular momentum) for which fusion occurs.

In this paper we extend our previous studies of fusion reactions between fullerenes and give a full discussion of our experimental work concerning the three possible fusion reactions involving the fullerenes C_{60} and C_{70}. The energy dependences of the cross sections for the reactions $C_n^+ + C_m \longrightarrow C_{n+m}^+$ will be presented and discussed using phenomenological models. It will be shown that our experimental results are well predicted by published calculations. Accompanying QMD calculations are discussed in a separate article in this issue (Knospe *et al* 1996). In the following section our experimental set-up will be presented. In section 3 the results will be given, followed by a discussion in section 4. The paper ends with a conclusion in section 5.

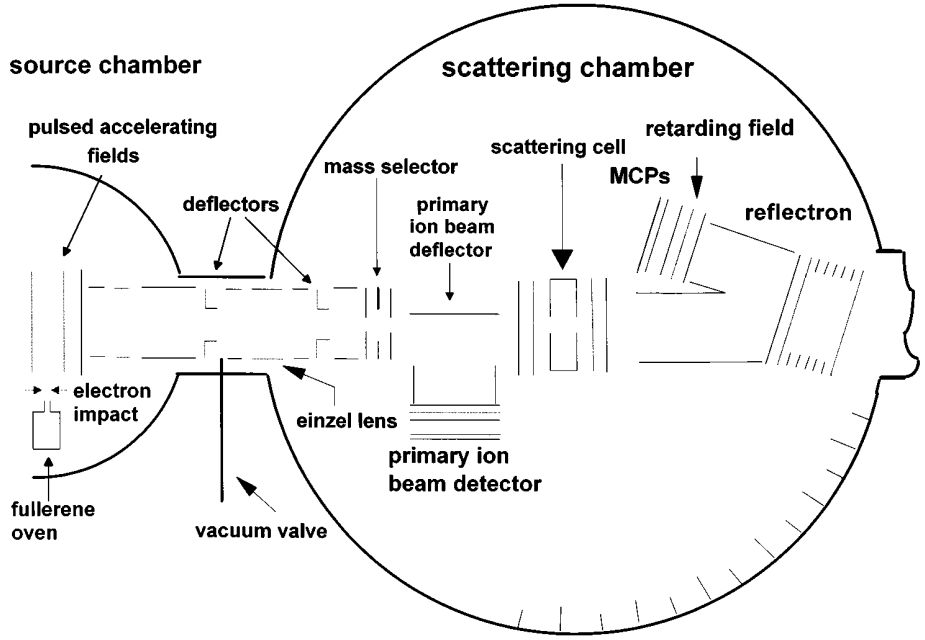

Figure 1. Experimental setup.

2. Experimental

The experimental set-up used for the CCC experiments is almost identical to that described previously (Rohmund and Campbell 1995). Our apparatus, which is depicted in figure 1, consists of two differentially pumped vacuum chambers. The source chamber contains the fullerene ion source and acceleration ion optics. The target cell and the detectors are located in the scattering chamber. During measurements, the background pressure in both chambers is in the range of 10^{-7} mbar or better. Fullerene ions are produced by vaporizing a home-made mixture of approximately 90% C_{60}, 10% C_{70} and traces of higher fullerenes in a resistively heated oven with subsequent electron impact ionization. The ions drift into

the region between two acceleration electrodes. A pulsed electric field is applied to these electrodes, accelerating the ions into the scattering chamber. A mass selector is situated in front of the scattering cell. It consists of a thin metal wire, placed between two wire meshes, which crosses the ion path and is set on a positive potential to deflect the ions coming from the source chamber. By switching the voltage on this wire to zero for a short time (typically 0.4 to 1.2 μs) at an appropriate delay with respect to the pulsed acceleration field in the source chamber, only ions of the desired mass-to-charge ratio are allowed to fly unhindered towards the scattering cell. The intensity of the primary ion beam is monitored by a switched electrostatic beam deflector and a pair of multichannel plates (MCPs), located after the mass selector and before the scattering cell. The scattering cell is situated in the middle of the scattering chamber. It is a cylindrical oven (20 mm long, 40 mm diameter) in which C_{60} or C_{70} of high purity (99.4%, Hoechst 'Gold Grade') is vaporized. The ions enter the scattering cell through a circular orifice of 4 mm diameter. Both reaction products and the primary ions which suffered no collision leave the scattering cell through a second identical orifice and drift through a field free region before they enter a reflectron. After exiting the reflectron and passing through a second field free region the ions are detected by a pair of MCPs. The total acceptance angle is limited by the reflectron and is 1.2°.

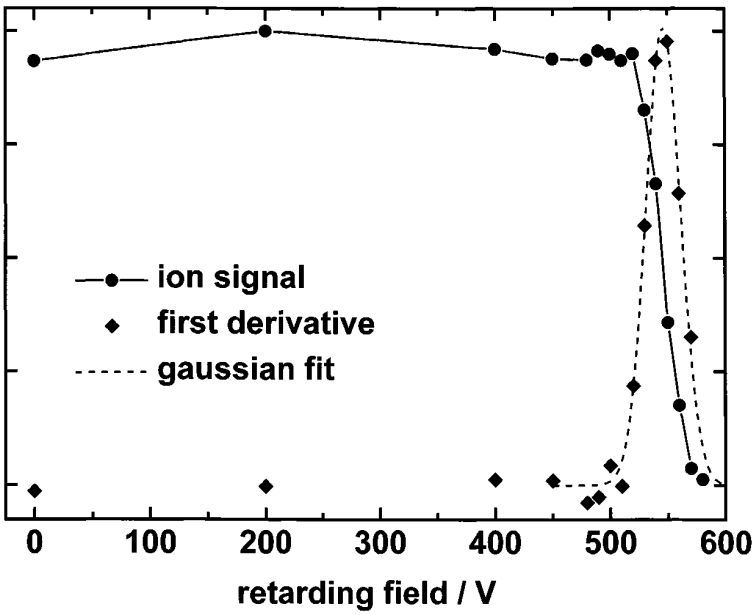

Figure 2. Attenuation of the ion signal by the retarding field in front of the MCP detector of the reflectron. From the derivative of the signal and a Gaussian fit the mean (lab-) energy E_{lab} and the width Γ_{lab} of the energy distribution can be obtained. For the example shown, $E_{\mathrm{lab}} = 540$ eV, $\Gamma_{\mathrm{lab}} = 30$ eV. Note that apart from this figure all energies given throughout this paper are related to the centre-of-mass frame.

A retarding field analyser is located in front of the reflectron MCPs. It is used to determine the kinetic energy distribution of the reflected ions. Figure 2 shows a typical dependence of the signal of C_{60}^{+} ions on the retarding field. The signal is nearly constant until it drops abruptly around a retarding potential of 540 V. Also included in figure 2 is the first derivative of the ion signal, scaled appropriately, and a Gaussian fit to it. From this fit

we get both the most probable ion energy E and the FWHM, Γ of the energy distribution. For the example given in figure 2, $E_{\mathrm{lab}} = 540$ eV and $\Gamma_{\mathrm{lab}} = 30$ eV.

For the determination of fusion cross sections the mass spectra had to be corrected with respect to the mass-dependent detection efficiency of the MCP detector. As described elsewhere (Rohmund and Campbell 1995), the ion signal depends exponentially on the ion velocity v at the surface of the first MCP

$$I = I_0 \exp[b(v - v_0)] \tag{1}$$

at least in the range of ion velocities between approximately 2.5 and $4.5 \times 10^4\,\mathrm{m\,s^{-1}}$ of our experiment. Here I_0 is the intensity measured at an impact velocity v_0 and $b = 1.2(2)10^{-4}\,\mathrm{s\,m^{-1}}$ is an experimentally determined parameter. Figure 6 shows a mass spectrum before and after correction. In our experiment v_0 is the impact velocity of the C_{60}^+ or C_{70}^+ primary ion. As can be seen from this plot, the influence of the detection efficiency is remarkable and cannot be omitted. The fairly large uncertainty in b is the main reason for the errors in the absolute values of the cross sections.

In contrast to our previous work (Rohmund and Campbell 1995), the collision energy is not changed by choosing different accelerating conditions in the source chamber. Instead, a positive voltage is applied to the scattering cell while the ion source conditions are kept constant. This has the advantage that during most of their flight time the ions drift with a relatively high kinetic energy (a typical acceleration voltage in the source is 540 eV), which reduces considerably problems with ion loss due to space charge effects or scattering from rest gas. The kinetic energy is relatively low only during passage through the scattering cell and its acceleration and deceleration ion optics (total length 74 mm, compared to the total flight length of 1.5 m). This set up made it possible to measure the fusion barriers, described in the following section, which lie below 200 eV in the laboratory frame.

The absolute signal of the fusion products is very low. We therefore used a digital multichannel scaler coupled with a discriminator for data acquisition which enables single ion counting. The primary ion beam, however, was recorded with a digital oscilloscope. The product signal could be normalized to the primary ion signal after calibration of the multiscaler signal to the oscilloscope signal at low ion intensities (where no saturation of the multiscaler signal occurred).

Fusion cross sections were determined by recording the fusion signal I_{fus} as a function of the temperature of the scattering cell and using the relation

$$I_{\mathrm{fus}} = I_0 n \sigma l \tag{2}$$

in the temperature range where single collision conditions are dominant (see section 3). Here σ is the cross section, n is the number density of the target gas and $l = 28$ mm is the effective length of the scattering cell. For the calculation of n we used parametrized vapour pressure curves from the literature. It should be noted here that there exist some discrepancies in the literature in the determination of the fullerene vapour pressure as a function of the temperature. We used the calibration curves of Abrefah *et al* (1992) and Mathews *et al* (1993) which nearly coincide in the temperature range of interest for C_{60}. However, Popovic *et al* (1994) published values of the fullerene vapour pressure which are approximately one order of magnitude larger than the results of the references mentioned above. Therefore application of (2) may introduce a considerable error in the determined fusion cross sections. All fusion cross sections calculated in this way from the experimental data were found to be much smaller than the geometric or total scattering cross section.

In contrast to the first CCC experiments (Campbell *et al* 1993), we do not use a laser desorption source for the production of the primary ions. The vaporization source used

enables us to carry out our measurements with much higher repetition rates (1 kHz compared to 10 Hz), which drastically reduces the measuring time.

Laser desorbed ions have very high internal energies (Mitzner and Campbell 1995). Vaporization of fullerenes with subsequent electron impact ionization may, under certain conditions, be expected to produce colder ions. However, for our experimental set-up we gave an upper limit for the temperature of the projectile of 2400 K (Rohmund and Campbell 1995), which is only slightly smaller than the values obtained for laser desorption (Mitzner and Campbell 1995). On the other hand, the internal energy of the target molecules is determined by the temperature of the target cell which lies typically between 720 and 820 K. Therefore the average temperature of the colliding clusters is smaller than 2400 K.

3. Experimental results

Figure 3 shows four mass spectra from collisions of C_{60}^+ with C_{60} at a collision energy of 126 eV. In the figure the temperature of the scattering cell for each measurement is given. At $T = 365\,^{\circ}\mathrm{C}$, only primary ions C_{60}^+ can be seen. With increasing temperature a broad range of signal between 150 μs and 167 μs is detected. This signal is the result of fusion and subsequent fragmentation of the compound. Due to the length of our scattering cell mass peaks originating from different product ions are not clearly resolved. The flight time of the primary ions and the two limits on the flight times of the fusion products were simulated, the latter by taking into account that all the kinetic energy in the centre of mass frame is converted into internal energy if two clusters fuse. It was assumed that fragmentation of the fused C_{120}^+ occurs via evaporation of small fragments which do not significantly affect the flight path or translational energy of the product ions (we will show below that this is a reasonable assumption). The two dashed lines in figure 3 then indicate the range of the fusion products between C_{120}^+ and C_{60}^+, the dotted line the position of the smallest fusion product, C_{19}^+, which we should be able to detect under the experimental conditions. From the figure it is obvious that all fusion products have already undergone some evaporation or fragmentation on the timescale of our experiment at this collision energy.

The energy dependence of the fusion and fragmentation process can be seen in figure 4, where mass spectra for different collision energies are depicted. The dashed lines indicate the flight times of the product ions C_{120}^+ and C_{60}^+ as in figure 3. At the lowest collision energy shown, no fusion signal is visible. With increasing energy, signals due to fusion products and their fragments appear and increase before dropping to zero around $E = 200$ eV. With increasing energy the product distribution broadens and the average product size shifts to lower masses. At $E = 88.5$ eV signal from C_{120}^+ is still clearly visible. At 133.5 eV, only fragments can be detected.

In figure 5, the average product masses for all three types of collision experiments described here are plotted. The different collision experiments show a similar behaviour. The decrease in the average product mass is nearly linear up to a certain collision energy at which the average mass strongly decreases. This is more pronounced in the two experiments involving C_{70}. The lines in figure 5 are the results of a statistical evaporation model which will be discussed in detail in the next section.

Figure 7 shows how the total and corrected fusion signal (summed over all product masses) from a collision between C_{60}^+ and C_{60} depends on the target number density. A linear fit to the data (equation (2)) is also shown. Above a value of $n = 3 \times 10^{19}\,\mathrm{m}^{-3}$ deviations from linear behaviour arise. For this reason the linear fit has only been carried out to the number density indicated in the figure. After the measurement of the temperature dependence of the fusion signal at a fixed collision energy, the collision energy was varied

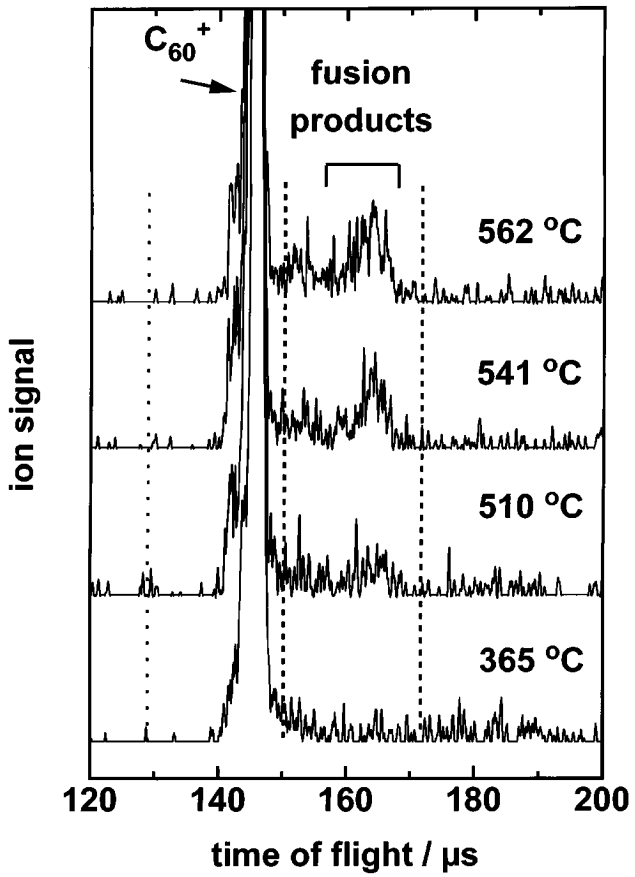

Figure 3. Mass spectra of collisions $C_{60}^{+} + C_{60}$ with an collision energy of 126 eV. From bottom to top the temperature of the scattering cell is increased. With rising target gas pressure in the scattering cell, the fusion signal between 150 and 167 μs increases. The dashed lines indicate the range of the fusion products C_{60}^{+} to C_{120}^{+}, the dotted line the flight time of the smallest fusion product C_{19}^{+} which should be possible to detect under the present experimental conditions.

under single collision conditions. From the relative values of the fusion signal and the temperature dependence for one energy the whole energy dependence of the fusion cross section has been obtained.

The energy dependences of the fusion cross section σ for the three sets of collision partners $C_{60}^{+} + C_{60}$, $C_{60}^{+} + C_{70}$ and $C_{70}^{+} + C_{70}$ are shown in figure 8. For each pair of collision partners there is a well defined range of collision energies, the fusion window, in which fusion is observed. The maximum value of σ was observed to be 14 Å^2 for $C_{70}^{+} + C_{70}$ collisions. With increasing total number of atoms participating in the fusion process the minimum energy under which fusion occurs, the maximum value of σ and the width of the fusion window increase. We carried out the fusion experiment between C_{60} and C_{70} with both C_{60} and C_{70} as projectile ion and C_{70} and C_{60} as target cluster, respectively. The results are, as one would expect, identical. We regard this as an indication of the reliability of our results. Data from both experiments are included in figure 8. The error bars given in these figures represent the reproducibility of the relative values. The absolute error of the

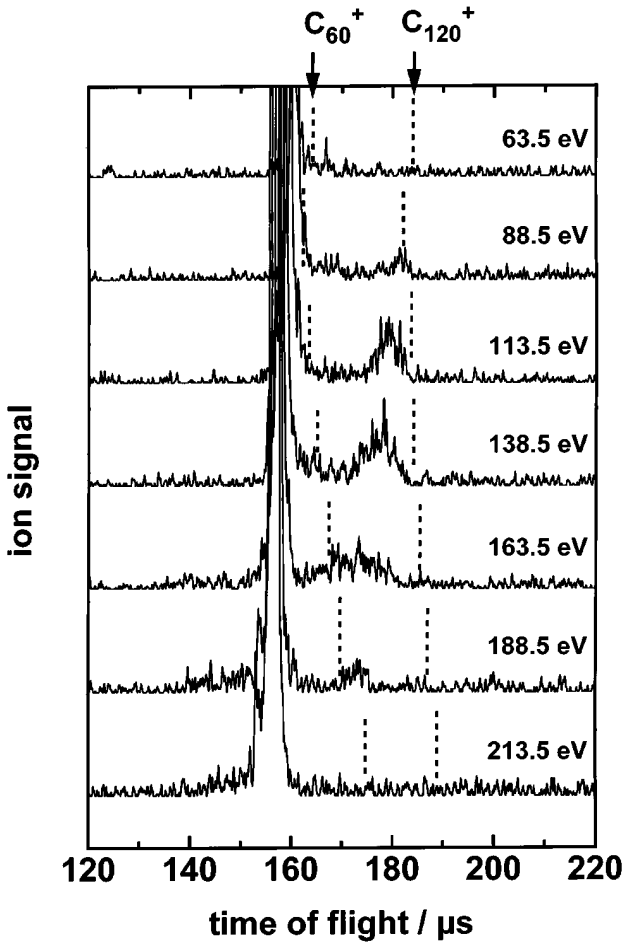

Figure 4. Mass spectra of collisions $C_{60}^{+} + C_{60}$ with different collision energies as indicated in the figure. At the lowest and the highest collision energy shown, no signal arising from fused fullerenes is visible. Beyond the fusion threshold the product ion distribution broadens and shifts to lower masses if the collision energy is increased.

values of σ is in the range of 50%.

4. Discussion

4.1. Fusion

Two simple phenomenological models for the fusion reaction have been applied to extract quantitative information from the measured energy dependences of the fusion cross section. Both are derived and described in more detail by Knospe *et al* (1996).

The simplest ansatz, already applied in the previous report (Rohmund *et al* 1996), is the absorbing sphere model (ASM). It assumes that fusion occurs if the impact parameter is smaller than or equal to the geometrical cross section πR_{12} and the collision energy E is equal to or larger than the fusion barrier V_b plus the centrifugal barrier. These assumptions

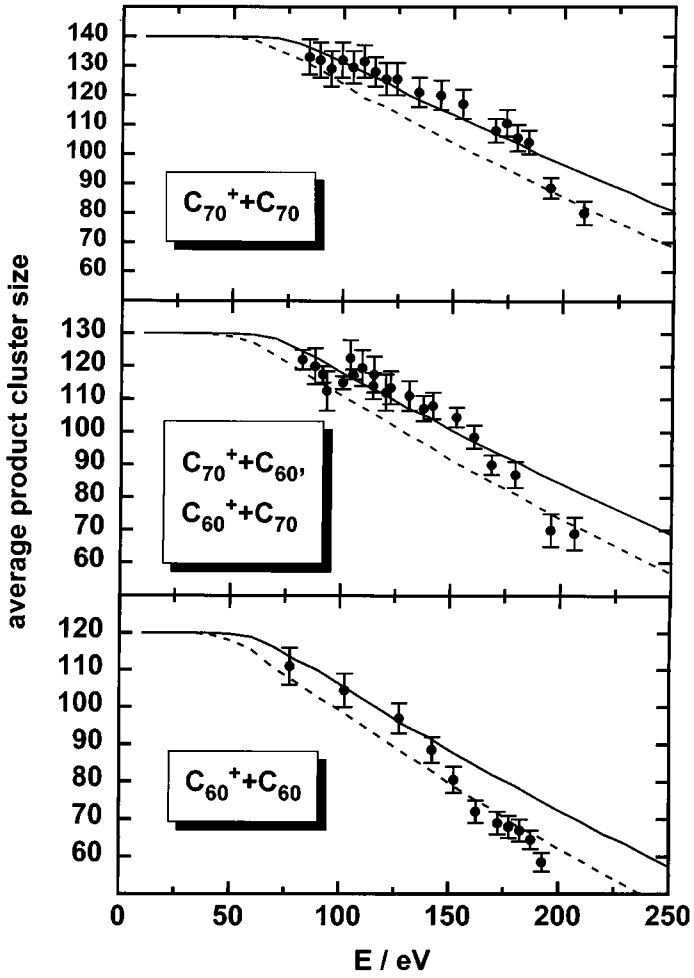

Figure 5. Average fusion product size as a function of the collision energy for the different collision systems. Symbols: experimental values. Lines: calculations assuming successive evaporation of C_2 units (see text for details). Two different dissociation energies have been applied: 6.4 eV (full) and 5.6 eV (dashed).

lead to the fusion cross section

$$\sigma = \bar{P}\pi R_{12}^2 \left(1 - \frac{V_b}{E}\right). \tag{3}$$

The parameter $\bar{P}$ introduced here is the average probability for a fusion event after all the energetic and impact parameter constraints have been taken into account by the model. As we have shown previously for $C_{60}^{+} + C_{60}$ (Rohmund *et al* 1996) and will confirm below for the other collision partners, $\bar{P}$ is much smaller than one in the case of fullerene–fullerene collisions. The value of $\bar{P}$ is expected to be smaller than one due to steric factors hindering the fusion. We note in passing that the value of $\bar{P}$ which is determined below is similar in nature and magnitude to the *ad hoc* reduction in the rate introduced in equation (7).

Fits of equation (3) to the experimental values of σ have been calculated in the range

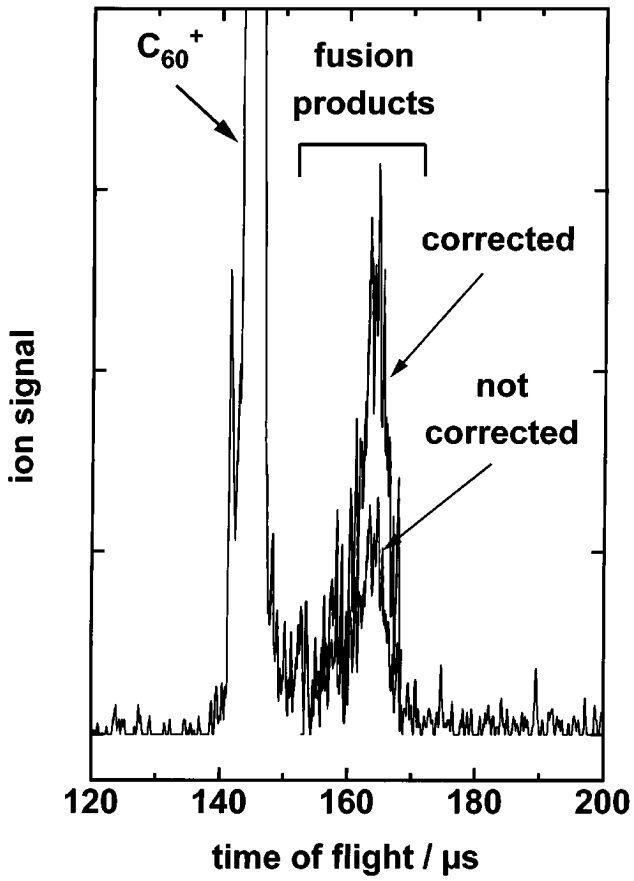

Figure 6. Raw and corrected mass spectrum of a collision $C_{60}^{+} + C_{60}$ with a collision energy of 126 eV. The correction has been carried out using the relation $I = I_0 \exp[b(v - v_0)]$.

of low collision energies. This is shown in figure 8. The model prediction from (3) is a dependence of σ on $1/E$ which is linear. However, deviations from the linear behaviour are visible for all three systems in the region of low energies, where the experimental points lie below the fitted lines. The extracted parameters $\bar{P}$ and V_b as well as the critical energy E_{cr} where the cross section reaches its maximum are summarized in table 1. The extracted fusion barriers V_b are relatively large. They increase with increasing size of the collision system and lie in the range between 67 and 85 eV. The barriers for the two collision systems involving C_{70} are nearly identical. For the fusion probability a more pronounced increase is observed. The values are 0.023 for $C_{60}^{+} + C_{60}$ but 0.08 and 0.176 for $C_{60}^{+} + C_{70}$ and $C_{70}^{+} + C_{70}$, respectively. Note that the uncertainties for both V_b and $\bar{P}$ are in the range of 10%.

If the collision energy E and the angular momentum l become larger than critical values E_{cr} and l_{cr}, respectively, (3) is not expected to be valid (Knospe *et al* 1996). In the range of larger collision energies the fusion cross section σ is expected to decrease according to

$$\sigma = \frac{\pi\hbar^2}{2\mu E} l_{cr}^2 \bar{P}. \tag{4}$$

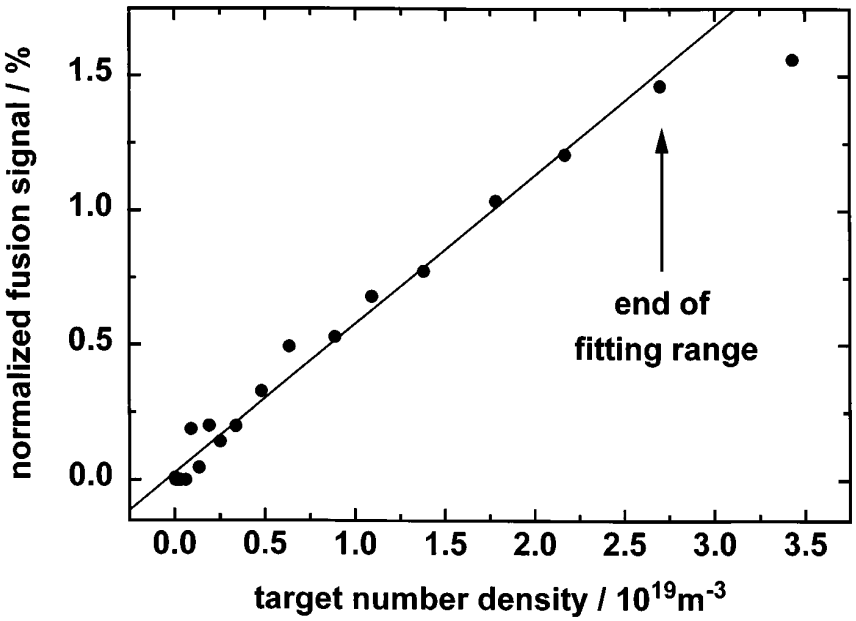

Figure 7. Total (corrected) fusion signal as a function of the target number density n for a fixed collision energy ($C_{60}^{+} + C_{60}$ 126 eV). From the linear fit to the data the total fusion cross section can be obtained.

Table 1. Summary of quantities extracted from the experimental dependences of the fusion cross section on the collision energy using the absorbing sphere model (ASM) and the steric model (SM). The uncertainties do not include systematic contributions.

Collision system	V_b^{ASM} (eV)	V_B^{SM} (eV)	P	E_{cr} (eV)	l_{cr}	b_{cr} (Å)	σ_{cr} (Å^2)
$C_{60} + C_{60}$	67(7)	60(1)	0.023(2)	138.5	$24\,500\hbar$	5.14	1.8
$C_{60} + C_{70}$	84(9)	70(7)	0.080(8)	137.7	$23\,000\hbar$	4.75	5.15
$C_{70} + C_{70}$	86(12)	76(4)	0.176(13)	144.6	$25\,900\hbar$	4.72	12.7

The corresponding lines are included in figure 8. Obviously, the observed signal decreases much stronger with E than predicted by (4). Note that for $\bar{P}$ the value obtained from the low energy regime, (3), has been used. From the critical fusion cross section σ_{cr} observed at the critical collision energy E_{cr} it is possible by application of (4) to calculate the critical angular momentum l_{cr} as well as the critical (i.e. maximum) impact parameter b_{cr}. These quantities are also given in table 1. l_{cr} is approximately $24\,000\hbar$, b_{cr} approximately 4.9 Å for all of the collision systems investigated here. Due to the relatively large errors of E_{cr} the deviations of the actual values given in table 1 from these mean values are not significant.

The simple ASM fits the experimental data quite well, and in particular allows us to extract a value for the fusion barrier from the data, however some deviations occur. For this reason we applied another model to our results which is basically an extension of the ASM. The additional assumption is that a steric factor is important in fusion dynamics, therefore we will refer to it as the steric model (SM) in the rest of the paper. As described in the companion paper (Knospe *et al* 1996), the fusion cross section should depend on the

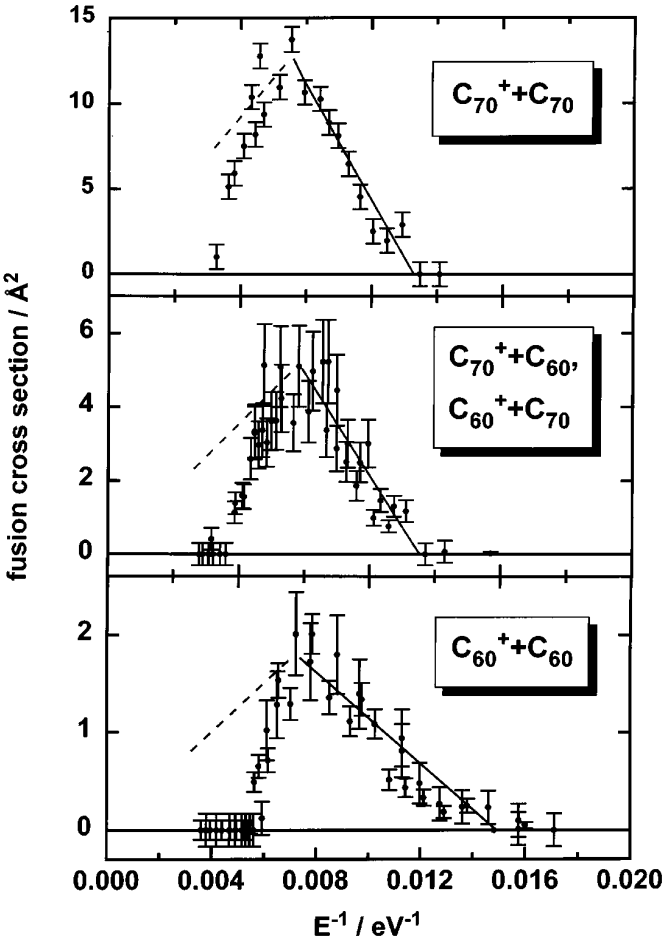

Figure 8. Dependences of the fusion cross section on the reciprocal collision energy for the different collision systems investigated. Symbols: experimental values. Dashed-dotted lines: linear fits according to the adsorbing sphere model in the low energy range; dashed lines: calculation of σ according to the absorbing sphere model in the high energy range beyond the onset of centrifugal fragmentation; full lines: fits according to the steric model in the low energy range.

collision energy as

$$\sigma = \sigma_0 \frac{(E - V_b)^2}{E}. \tag{5}$$

Equation (5) predicts an energy dependence of the fusion cross section with a positive curvature if it is plotted against E. That this is indeed the case is shown in figure 8. The agreement between the fits and the data is excellent. The fusion barriers extracted from the fitting routines are also given in table 1. They are smaller than those obtained with the ASM, but the relatively large error regions overlap. The difference in the fusion barriers between the two collision systems $C_{60}^{+} + C_{70}$ and $C_{70}^{+} + C_{70}$ is larger than that obtained with the ASM.

Irrespective of the model we use for the interpretation of the measured energy

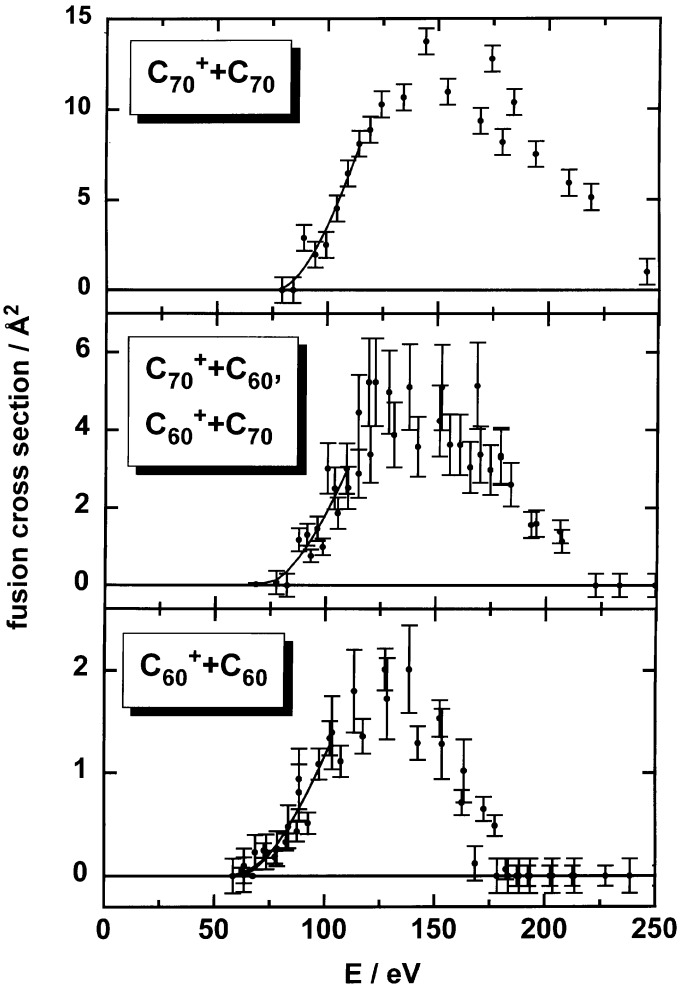

Figure 9. Energy dependence of the cross section for fusion of two C_{60} fullerenes. Symbols: experimental values; curve: fit to the data assuming the absorbing sphere model with an energy-dependent fusion probability $P = 0.5\{1 + \tanh[a(E - b)]\}$; $a = 0.0443$ eV, $b = 86.75$ eV.

dependences of the fusion cross sections, we obtain relatively large values for the fusion barrier V_b, in the range of several tens of eV. Thus the possibility of a van der Waals or polymer-like bonding between the two fullerenes in the fusion compound can be ruled out. For polymeric systems the activation barrier for dissociation has been shown experimentally to be 1.25 eV (Wang *et al* 1994). Therefore it is clear that in our experiment the cages of the colliding clusters are opened and a new compact or fullerene-like cluster is formed. During its formation many bonds have to be broken, giving rise to the large fusion barriers measured. This scenario is supported by the variety of theoretical investigations concerning non-thermal fusion reactions between two C_{60} fullerenes (Seifert and Schmidt 1992, Zhang *et al* 1993, Robertson *et al* 1995, Rohmund *et al* 1996). These studies show that the fusion compounds should indeed have a fullerene-like cage structure although not necessarily the most energetically stable isomer. For example, in the paper by Knospe *et al* in this volume,

a trend towards a peanut-like structure can be seen in the results of the QMD calculations.

The question of fusion barriers for two C_{60} clusters has been addressed theoretically for the experimental energy range relevant here by Zhang *et al* (1993) and Robertson *et al* (1995). The quantitative agreement between measured and calculated fusion barriers can be drawn from the analysis of our data using the ASM and the SM. The values for V_B given in table 1 are in the region of 60 eV. This is identical to the fusion barrier obtained from tight binding calculations (Zhang *et al* 1993) and classical MD (Robertson *et al* 1995) if a temperature of the reactants of about 2000 K is assumed. We will discuss the problem of the initial temperature in more detail below. In our previous report (Rohmund *et al* 1996) an upper limit of $V_B \approx 80$ eV was estimated from QMD calculations carried out at $T = 0$ K. Consideration of the internal excitation of the reactants is expected to yield a smaller value in the range of the experimental value. This is indeed the case as shown in the companion paper (Knospe *et al* 1996).

Some inferences about the fusion mechanism can be made from the way the fusion barrier varies with collision partners. We showed in section 3 that V_B increases with increasing number of atoms included in the collision process. Two qualitative explanations can be suggested for this behaviour. Firstly, one may attempt to treat the fusion as a completely statistical process. Then, when the number of atoms and therefore the number of degrees of freedom in a cluster is increased, the energy necessary to open the fullerene cage is also increased. If this is true, the increase in V_b between the three collision systems, from $C_{60}^+ + C_{60}$ through $C_{60}^+ + C_{70}$ to $C_{70}^+ + C_{70}$ fusion, should be similar. It is, however, observed that the fusion barriers for the two experiments including C_{70} are nearly identical, whereas the value for $C_{60}^+ + C_{60}$ collisions is considerably smaller. Another argument against the model is theoretical; if a statistical process is needed to open the cage, the equilibration of the excitation energy during the collision must be faster than the breaking of the bonds. QMD-calculations, however, show that the bond breaking in the contact zone of the colliding clusters is faster than the energy equilibration. Therefore the explanation of statistical opening of the cluster bonds can be ruled out. Another explanation of the increase of V_b might be the different (lower) symmetry of C_{70} compared to C_{60}. From our experiments alone no information concerning this question is obtainable. Although experiments have been interpreted in terms of participant/spectator regions of the colliding molecules (Mowrey *et al* 1992), these collisions could be so different from ours, that we may have to await further theoretical investigations in order to clarify this point.

The fusion cross section can be described quite satisfactorily by the ASM in the low energy region (equation (3)). Besides the fusion barriers given in table 1 the average probabilities $\bar{P}$ for fusion can be extracted from the fit parameters. The values of $\bar{P}$ are very low. They are found to be in the range between 2% and 18%. This is in contrast to fusion processes in HIC (Bock 1980) and collisions between sodium clusters (Schmidt et al 1991) where fusion probabilities of (nearly) 1 are observed or, in the latter case, expected. The experimental value of $\bar{P}$ can be compared with results from QMD calculations. As reported earlier (Rohmund et al 1996) the estimated $\bar{P}$ for the fusion of two C_{60}s is 0.057. The agreement between this theoretical value and the experimental result of $\bar{P} = 0.023$ is good if one takes into account the quite large uncertainties in the experiments and the limited number of trajectories from the QMD calculations. The reason for the low value of $\bar{P}$ is the strong dependence of the reaction channel on the orientation of the two reactants. Different reaction channels are open at the same collision energy for collisions between fullerenes. In the range of energies important for this study, QMD predicts fusion, deep inelastic scattering and fragmentation as competing processes (Rohmund *et al* 1996). The reaction path actually chosen in a collision depends sensitively on the orientation of the

collision partners, even if the impact parameter is the same. Furthermore, not all the centre-of-mass kinetic energy is converted into heat during the collision but a substantial amount is stored in potential energy. An additional characteristic of fullerene–fullerene collisions is that the collision partners separate again from each other in a 'bouncing off' mechanism which also serves to lower $\bar{P}$ (Rohmund *et al* 1996).

The dependence of the reaction channel chosen in a CCC and the fusion probability P on the orientation of the reactants motivated us to apply the SM with the fusion model cross section given in (5). From comparison of (3) and (5) it can be seen that a fusion probability P which increases linearly with increasing collision energy is included in the SM. Such a behaviour is reasonable for fusion of fullerenes because at higher collision energies a larger variety of orientations of the reactants is expected to lead to fusion and therefore P should rise. The fitting parameter σ_0 in (5) is given by $\sigma_0 = \alpha\pi R_{12}^2$ (Knospe *et al* 1996). The parameter α is determined by the dependence of the fusion barrier on the orientation of the reactants and has the dimension of a reciprocal energy. It can be extracted from the fitted value of σ_0 but for fusion reactions of fullerenes its physical meaning is unclear. Nevertheless the fitted curves shown in figure 8 are in excellent agreement with the experiment confirming the basic assumption of a linearly increasing fusion probability in the SM.

The probability for the fusion of two C_{60} fullerenes for zero impact parameter was calculated explicitly using classical MD as a function of the temperature of the reactants and the collision energy by Robertson *et al* (1995). For each temperature they fitted the fusion parameter P. Introducing their fit function into (3), $\bar{P} = P$ yields

$$\sigma = 0.5\{1 + \tanh[a(E-b)]\}\pi R^2 \left(1 - \frac{V_B}{E}\right). \tag{6}$$

We fitted our experimental results of the cross section for fusion of two C_{60}s with (6). The result is depicted in figure 9. The agreement between experiment and the fitted curve is excellent. Beyond the maximum value for σ the experimental data deviate from the fitted curve due to the fragmentation at high collision energies which is not taken into consideration in (6). From the fitting procedure the four fit parameters a, b, V_b and $\sigma_0' = \pi R^2$, given in table 2, are obtained. As can be seen from comparison with table 1, σ_0' and V_B are similar to the results obtained for $\bar{P}\pi R_{12}^2$ from the ASM and for V_B from the SM, respectively (note the large errors from the fitting routine). Direct comparison of a and b with results given in the publication of Robertson *et al*, also listed in table 2 for some selected temperatures, yields a temperature T of the reactants between 1800 and 2000 K. It will be discussed below that these values for T are reasonable. The connecting line between (6) and the SM can be drawn by use of the approximation $\tanh x \approx x$ for small x. For $a \approx 4 \times 10^{-2}\,\mathrm{eV}^{-1}$ and $b \approx 87$ eV (cf table 2) this approximation is valid for collision energies between 75 and 100 eV. With this substitution a linear increase of P with increasing collision energy is obtained from (6) similar to the SM. From the very good agreement between (6) and the experiment we therefore conclude that the SM is more reliable for a quantitative analysis of our data than the ASM.

As mentioned above Robertson *et al* calculated P for zero impact parameter only. As a consequence the fitting parameter σ_0' is much smaller than the geometrical cross section and close to the value of $\bar{P}\pi R_{12}^2$ from the ASM. The fact that the experimental data can be reproduced by (6) so nicely gives us a hint that mainly central collisions lead to fusion. This is also confirmed by the small values of σ compared to the geometrical cross sections for all fusion reactions investigated here. The geometrical cross sections for the collisions $C_{60} + C_{60}$, $C_{70} + C_{60}$ and $C_{70} + C_{70}$ are given by 154, 166 and 179 Å^2, whereas the

Table 2. Fitting parameters obtained from application of (6) for fusion of two C_{60} fullerenes (figure 9). Values from MD calculations (Robertson *et al* 1995) for the parameters a and b are also listed for comparison.

	σ_0' (Å^2)	V_B (eV)	a (10^{-2} eV^{-1})	b (eV)
Experiment	3.4(1.1)	57(22)	4.4(1.4)	87(12)
MD, $T = 1800$ K			4.3	95.4
MD, $T = 2000$ K			4.9	87.6

maximum fusion cross sections are 2, 5.2 and 14 Å^2, respectively. Thereby the fusion probability P should strongly depend on the impact parameter b. P should peak at $b = 0$ and drop sharply to zero if b exceeds a certain energy dependent value b_{cr}.

The width of the fusion window increases with the number of atoms in the fusion process. The FWHMs obtained from the energy dependences of σ are 64, 78 and 97 eV for the collisions $C_{60}^+ + C_{60}$, $C_{60}^+ + C_{70}$ and $C_{70}^+ + C_{70}$, respectively. This increase is reasonable because a larger compound cluster can store more internal energy due to the higher number of degrees of freedom. The absolute increase of the width of the fusion window is, however, larger than expected by a linear scaling with the number of degrees of freedom.

One important point mentioned several times throughout this paper is the internal excitation E_0 of the reactants before the collision. The amount of E_0 has a direct impact on the fusion barrier and on the fragmentation behaviour of the fusion product. Whereas the internal energy of the target cluster is determined by the temperature of the scattering cell (for a typical temperature of 500 °C a value of 3.1 eV can be calculated from (8), see section 4.2) it is not clear how much energy is put into the projectile by the electron impact. As discussed above, from comparison with theoretical results (Zhang *et al* 1993, Robertson *et al* 1995) a temperature of the reactants between 1800 and 2000 K can be estimated. The resulting total internal energy from these temperatures is between 36.9 and 42.6 eV. On the other hand, from the calculation of the successive evaporation of C_2 units from the fusion compound discussed in detail in the next section a total internal energy for both projectile and target cluster of 25 ± 10 eV is obtained. Both methods for the estimation of the internal energy are indirect and therefore the approximate agreement of the results can be regarded as quite satisfactory.

4.2. Fragmentation

In order to understand how the fragmentation pattern of the fusion products evolves with energy, we have simulated the destiny of these hot compounds with a Monte-Carlo calculation of their evaporative decay. We modelled the decay by successive loss of C_2 units from the fusion product. Such a mechanism has been shown to be dominant for the dissociation of excited fullerenes of different sizes and for different methods of excitation with moderate excitation energies (see e.g. Foltin *et al* 1993, O'Brien *et al* 1987, Beck *et al* 1996, Ehlich *et al* 1996). However, if the excitation energy exceeds a certain (size dependent) value, evidence for opening of other decay channels like fission into large fragments, has been observed (Hohmann *et al* 1994, Beck *et al* 1996). For the decay rate constant we used a simple Arrhenius expression

$$k = A \exp[-D/kT]. \tag{7}$$

Here D is the dissociation energy, T the temperature (see below) and k the Boltzmann constant. The pre-exponential factor was set to $A = 7.4 \times 10^{14}$ Hz in all cases. This

value is smaller than a typical pre-exponential from a detailed balance calculation using the absorbing sphere approximation and standard parameters for C_{60} which would be higher than $10^{16}\,s^{-1}$. The smaller value takes into account the steric factors reducing the cross section or, equivalently in the RRKM picture, the available phase space in the outgoing channels. As expected from ensemble considerations the results of the simulations are insensitive to the precise choice of this value. Changing the number by an order of magnitude produced almost the same results. The temperature T is defined in terms of the internal energy of the molecule by the Einstein crystal relation

$$E_i = \frac{(3n-6)h\nu}{\exp\left[h\nu/kT\right]-1} \approx (3n-6)[kT - \tfrac{1}{2}h\nu] \tag{8}$$

if we assume that all the centre-of-mass kinetic energy E plus the internal energy E_0 before the collision is stored in the vibrational degrees of freedom of the fused cluster, i.e. $E_i = E + E_0$. The last approximate relation, which has not been used in the simulations, holds for high temperatures. The rotational energy should be treated separately, since it is related to a conserved quantity, namely the angular momentum. For our present purposes we have neglected it. The average frequency ν of the harmonic vibrations of C_n^+ is unknown. For simplicity we used the value for C_{60}, $\nu = 2.7 \times 10^{13}$ Hz (Stanton and Newton 1988). In the calculations presented here the source energy, E_0, was set to 25 eV. This value yields the best agreement with the experimental results, but changes of E_0 of ± 10 eV do not influence the output of the computations dramatically. We did not specifically take into account any change in total cohesive energy upon fusion. This is reasonable since the binding energies of the fusion products relative to C_{60} lie in the range from 2.2 to –7.2 eV, as calculated by Strout *et al* (1993) for the peanut-like structures that are the most likely products of the collision (Knospe *et al* 1996). Such small values have no significant influence on the results of our calculations. The successive evaporation mechanism is realized using a Monte-Carlo algorithm. The internal energy for the specific molecule in a decay chain is converted to a rate using the above relations. This rate is then used to find a stochastic lifetime for the decay of a molecule C_n^+ into the product C_{n-2}^+ by the evaporation of a C_2 molecule. The lifetime is exponentially distributed with a mean value equal to the inverse of the rate and is generated by standard methods (see for example Abramowitz and Stegun 1970). The only effect of evaporation is to reduce the mass and the internal energy of the molecule. The internal energy of C_{n-2}^+ is given by that of C_n^+ reduced by the sum of the dissociation energy D and the kinetic energy release and internal energy of the C_2. The latter contributions were simply summed up to the fixed value of $2kT$. Thus, once the initial energy, the collision energy and the dissociation energy are fixed, all decay cascades in a simulation have a fixed set of decay rates. The stochastic element is then exclusively due to the stochastic nature of the decay times. A single decay chain terminates at a prescribed simulation time, which is chosen to be the experimentally relevant time. The mass of the simulated particles at this time is then averaged over the decay chains.

The important simulation factors that determine this averaged product mass are the initial energy content of the participators, the energy deposited into the fusion product on collision and the dissociation energy. In discussing the precise value of the initial, and the deposited energies, it should be noted that a change in these quantities of, for example 5 eV, only changes the value of the averaged product by one C_2 unit.

The average product masses calculated in this way are shown as lines in figure 5. For each collision system the two dissociation energies 5.6 eV (dashed lines) and 6.4 eV (full lines) were used. In the region of low collision energies the experimental values are well reproduced by the calculations assuming $D = 6.4$ eV, whereas at higher collision energies

$D = 5.6$ eV yields better agreement. The values of the dissociation energies for these two curves are given roughly by (minus) the inverse slope of the almost linear decreasing part of the simulation curves. The two values of D are rather close, separated by only 0.8 eV, and they are also similar to values often quoted for dissociation energies of smaller fullerenes with similar internal energies (e.g. Foltin *et al* 1993).

The experimental trend towards smaller product sizes than predicted by the Monte-Carlo calculations at higher collision energies may be an indication of increasing efficiency of other fragmentation channels apart from C_2 evaporation. The presence of alternative fragmentation channels through emission of heavier fragments will lower the apparent dissociation energy as will the presence of competing cooling channels such as radiative decay (Hansen and Campbell 1996). Our estimated values for the dissociation energy D can therefore only be taken as lower bounds and the small tendency in the experiment to a negative curvature may indicate that D for C_2 loss is slightly underestimated. Continuing to even higher energies, one can also expect the production of larger fragments from very highly excited fusion compounds (Schmidt *et al* 1994). If such larger fragments are produced in an explosive 'multi-fragmentation' process, imparting large transverse momenta to the products, we would not expect to be able to detect them efficiently with our acceptance angle of $\pm 0.6^\circ$. We believe this is the explanation for the fact that beyond collision energies between 200 and 220 eV *no* fusion products at all are detected anymore. Measurements of angular distributions of the products should help to clarify the situation.

Interestingly, preliminary results on the internal energy dependence of the fragmentation of C_{120}^+ using a maximum entropy model, as has recently been applied to C_{60} (Campbell *et al* 1996), predict the onset of a phase transition leading to the production of small charged cluster fragments ($n < 30$) for an internal energy of approximately 200 eV. This will be the subject of further investigations.

5. Conclusion

In this paper we have presented detailed experimental results for the collisional energy dependence of the fusion cross sections for the systems $C_{60}^+ + C_{60}$, $C_{60}^+ + C_{70}$ and $C_{70}^+ + C_{70}$. The energetic barriers for the fusion reactions are in very good agreement with the predictions of molecular dynamics simulations. The energy dependence of the cross sections can be very well understood by combining QMD with simple phenomenological models (Knospe *et al* 1996).

The fragmentation behaviour of the fusion products can be modelled by assuming C_2 evaporation up to an excitation energy of approximately 200 eV. Beyond this value a different fragmentation mechanism, possibly involving the production of multiple fragments on a short time scale—related to the onset of a phase transition—seems to be occurring.

Acknowledgments

The work presented here benefited very much from an ongoing collaboration with our colleagues O Knospe, G Seifert and R Schmidt from the Technische Universität Dresden. The financial support by the Deutsche Forschunggemeinschaft through SFB 337 'Energie- und Ladungsaustausch Molekularer Aggregate' and by the European Union through HCM Network 'Formation, Stability and Photophysics of Fullerenes' is gratefully acknowledged.

References

Abramowitz M and Stegun I 1970 *Handbook of Mathematical Functions* (New York: Dover)
Abrefah J, Olander D R, Balooch M, Siekhaus W J 1992 *Appl. Phys. Lett.* **60** 1313
Basir Y, Wan Z, Christian J F, Anderson S L 1994 *Int. J. Mass Spectrom. Ion Proc.* **138** 173
Beck R D, Rockenberger J, Weis P and Kappes M M 1996 *J. Chem. Phys.* **104** 3638
Beck R D, St John P M, Alvarez M M, Diederich F, and Whetten R L 1991 *J. Phys. Chem* **95** 8402
Blaisten-Barojas E and Zachariah M R 1992 *Phys. Rev.* B **45** 4403
Bock R 1980 *Heavy Ion Collisions* vols 1–3 (Amsterdam: North-Holland)
Brenn G and Frohn A 1989 *Exp. Fluids* **7** 441
Caldwell K A, Giblin D E, Gross M L 1992 *J. Am. Chem. Soc.* **114** 3743
Campbell E E B, Raz T and Levine R D 1996 *Chem. Phys. Lett.* **253** 261
Campbell E E B, Schyja V, Ehlich R and Hertel I V 1993 *Phys. Rev. Lett.* **70** 263
Christian J F, Wan Z and Anderson S L 1992 *J. Phys. Chem.* **96** 3574
Ehlich R, Westerburg M and Campbell E E B 1995 *J. Chem. Phys.* **104** 1900
Foltin M, Lezius M, Scheier P and Märk T D 1993 *J. Chem. Phys.* **98** 9624
Guilleumas M, Garcias F, Barranco M, Pi M and Suraud E 1993 *Z. Phys.* D **25** 227
Guilleumas M, Pi M, Barranco M and Suraud E 1995 *Z. Phys.* D **34** 35
Hansen K and Campbell E E B 1996 *J. Chem. Phys.* **104** 5012
Hohmann H, Callegari C, Furrer S, Grosenick D, Campbell E E B and Hertel I V 1994 *Phys. Rev. Lett.* **73** 1919
Javahery G, Petrie S, Wang J and Bohme D K 1992 *Int. J. Mass Spectrom. Ion Proc.* **120** R5
Knospe O, Glotov A V, Seifert G and Schmidt R 1996 *J. Phys. B: At. Mol. Opt. Phys.* **29** 5163–74
Lill T, Busmann H-G, Reif B, Hertel I V 1992 *Appl. Phys.* A **55** 461
Lill T, Lacher F, Busmann H G and Hertel I V 1993 *Phys. Rev. Lett.* **71** 3383
Martin T P, Näher U, Schaber H and Zimmermann U 1993 *Phys. Rev. Lett.* **70** 3079
Mathews C K, Sai Baba M and Lakshmi Narasimhan T S 1993 *Fullerene Sci. Technol.* **1** 101
Mathews C K, Sai Baba M, Lakshmi Narasimhan T S, Balasubramanian R, Sivaraman N, Srinivasan T G and Vasudeva Rao P R 1992 *J. Phys. Chem. 96* 3566
Mitzner R and Campbell E E B 1995 *J. Chem. Phys.* **103** 2445
Mitzner R, Winter B, Kusch Ch, Campbell E E B and Hertel I V 1996 *Z. Phys.* D **37** 89
Mowrey R C, Ross M M and Callahan J H 1992 *J. Phys. Chem.* **96** 4755
O'Brien S C, Heath J R, Curl R F and Smalley R E 1987 *J. Chem. Phys.* **88** 220
Popovic A, Drazic G and Marsel J 1994 *Rapid Commun. Mass Spectrom.* **8** 985
Robertson D H, Brenner D W and White C T 1995 *J. Phys. Chem.* **99** 15721
Rohmund F and Campbell E E B 1995 *Chem. Phys. Lett.* **245** 237
——1996 to be published
Rohmund F, Campbell E E B, Knospe O, Seifert G and Schmidt R 1996 *Phys. Rev. Lett.* **76** 3289
Scheidemann A A, Kresin V V and Knight W D 1994 *Phys. Rev.* A **49** R4293
Schmidt R and Lutz H O 1992 *Phys. Rev.* A **45** 7981
——1993 *Phys. Lett.* **183A** 338
Schmidt R, Schulte J, Knospe O and Seifert G 1994 *Phys. Lett.* **194A** 101
Schmidt R, Seifert G and Lutz H O 1991 *Phys. Lett.* **158A** 231
——1992 *Nuclear Physics Concepts In The Study Of Atomic Clusters* ed R Schmidt, H O Lutz and R Dreizler (Berlin: Springer) p 128
Schulte J, Knospe O, Seifert G and Schmidt G 1995 *Phys. Lett.* **198A** 51
Seifert G and Schmidt R 1992 *Int. J. Mod. Phys.* B **6** 3845
Shen H, Hvelplund P, Mathur D, Barany A, Cederquist H, Selberg N and Lorentz, D C 1995 *Phys. Rev.* A **52** 3847
Stanton R E and Newton M D 1988 *J. Phys. Chem.* **92** 2141, values for n have been scaled by a factor of 0.88
Strout D L, Murry R L, Xu C, Eckhoff W C, Odom G K and Scuseria G 1993 *Chem. Phys. Lett.* **214** 576
Yeretzian C, Beck R D and Whetten R L 1994 *Int. J. Mass Spectrom. Ion Proc.* 135 79
Yeretzian C, Hansen K, Diederich F and Whetten R L 1992 *Nature* **359** 44
Wan Z, Christian J F, Anderson S L 1992 *Phys. Rev. Lett.* **69** 1352
Wang Y, Holden J M, Bi X and Eklund P C 1994 *Chem. Phys. Lett.* **217** 413
Weiske, T, Bohme D K, Hrusak J, Krätschmer W, Schwarz H 1991 *Angew. Chem.* **103** 898
Zhang B L, Wang C Z, Chan C T and Ho K M 1993 *J. Phys. Chem.* **97** 3134
Zhang F S, Suraud E, Spiegelmann F, Frayssé V, Chatelin F and Glowinski R 1995 *Z. Phys.* D **35** 131